PAPER

Check for updates

Achieving efficient and stabilized organic solar cells by precisely controlling the proportion of copolymerized units in electron-rich polymers†

Qian Xie,‡[a,b,f] Yongjie Cui,‡[b,c] Zeng Chen,‡[d] Ming Zhang, [ID][e] Chao Liu,[f] Haiming Zhu,[d] Feng Liu, [ID][e] Christoph J. Brabec,[f] Xunfan Liao [ID] *[b] and Yiwang Chen [ID] *[b]

A series of random polymers based on the donor polymer PM6 were designed from the perspective of regulating the surface electrostatic potential (ESP) distribution of the polymers and applied in organic solar cells (OSCs). Random polymers with different ESPs were obtained by introducing structural units of polymer PM6 into the polymer structure as the third unit. The simulation results showed that the random polymers feature a wider electron-donating region after the introduction of BDT units, indicating a more efficient charge generation probability. Benefiting from the optimized morphology of the active layer and the stronger interaction between the donor and the acceptor in the active layer, the device exhibited the best charge transport efficiency and lower charge recombination after the introduction of 5% BDT units, and a high power conversion efficiency (PCE) of 16.76% was achieved. In addition, OSC devices based on random polymers incorporating 5% BDT units exhibit excellent device stability. In contrast, the devices based on random polymers after the introduction of BDD units showed a much lower PCE of around 13% due to the inferior charge generation and charge transport. This work not only provides a new perspective for the molecular design of efficient random polymers, but also demonstrates that the OSC devices based on random polymers can still achieve better stability.

1. Introduction

Organic solar cells (OSCs), as promising solar photovoltaic devices, possess the advantages of light weight, room temperature solution processing and the potential of fabricating flexible devices.[1–6] In recent years, the power conversion efficiencies (PCEs) of OSCs have improved to 19% with the advancement of molecular engineering and device optimization.[7–10] In order to further improve the PCE, the design and synthesis of new active layer materials becomes a crucial aspect.[11–14] However, despite the continuous updating and iteration of acceptor materials,[15–20] the development of polymer donor materials is constrained by the problems of the almost saturated monomer structure skeleton, high development cost of new structural units, and poor matching with Y-series acceptors.

As an effective and reliable method to address these issues, the random copolymerization strategy has been widely used to modify high performance polymer donor materials, and achieve high PCEs of over 17%.[21–24] By controlling the properties and the proportion of the third unit, optoelectronic properties such as the energy level, absorption spectrum, aggregation, and crystallization of the target random polymer can be effectively tuned.[25–27] In general, after determining the polymer matrix to be modified, the performance parameters of the OSCs based on it will be analyzed first to determine the direction of key modification. Secondly, optimization of the molecular configuration is also the focus of attention, for example, the third unit is introduced to improve the co-planarity of polymer molecules, so as to improve the carrier mobility.

[a]*Institute of Applied Chemistry, Jiangxi Academy of Sciences, Nanchang 330096, China*

[b]*National Engineering Research Center for Carbohydrate Synthesis/Key Lab of Fluorine and Silicon for Energy Materials and Chemistry of Ministry of Education, Jiangxi Normal University, 99 Ziyang Avenue, Nanchang 330022, China. E-mail: xfliao@jxnu.edu.cn, ywchen@ncu.edu.cn*

[c]*State Key Laboratory for Modification of Chemical Fibers and Polymer Materials, Donghua University, Shanghai 201620, China*

[d]*State Key Laboratory of Modern Optical Instrumentation, Key Laboratory of Excited State Materials of Zhejiang Province, Department of Chemistry, Zhejiang University, Hangzhou, Zhejiang 310027, China*

[e]*School of Chemistry and Chemical Engineering, Shanghai Jiaotong University, Shanghai 200240, China*

[f]*Friedrich-Alexander-Universität Erlangen-Nürnberg, Faculty of Engineering, Department of Material Science, Materials for Electronics and Energy Technology (i-MEET), Martensstraße 7, 91058 Erlangen, Germany*

†Electronic supplementary information (ESI) available. See DOI: https://doi.org/10.1039/d2nr03992c

‡These authors contributed equally to this work.

In addition, the morphology of the active layer can also be optimized by molecular design. However, the choice of the third unit has become a new challenge. Presently, the type of the third unit can be simply divided into four categories, as shown in Fig. S1,† but there is still no clear and reliable guideline.[28–35] Interestingly, the studies on surface electrostatic potential (ESP) interactions between donor and acceptor materials provide a perspective on the choice of the third unit. It has been reported that a larger difference in the averaged ESP values between the donor and acceptor materials is more conducive to the generation and transport of charges in the active layer.[36–38] In general, the ESP value of the acceptor material is positive, so if the donor material can reach a lower negative ESP value, more effective charge generation and transport can be achieved in the active layer.[39] In other words, if the ESP value of the donor material can be lower after introducing the third unit by random copolymerization, it will be a positive signal for more efficient charge generation and transport in the active layer. However, there are currently no studies focusing on the design of random polymers based on this viewpoint.

From the above analysis, two types of random polymers based on the high-efficiency polymer donor PM6 were designed. As shown in Fig. 1, structural building blocks of polymer PM6 (BDT and BDD units) were introduced into the polymer structure of PM6 as the third unit, respectively,

thereby realizing the difference in the composition ratio of the electron-donating unit and electron-withdrawing unit in the polymer structure. The simulation results showed that the random polymers tend to have a wider electron-donating region after the introduction of BDT units, indicating a more efficient charge generation probability. In addition, face-on molecular stacking with a longer crystalline coherence length was also obtained after the introduction of 5% BDT units, resulting in more efficient charge transport efficiency. Benefitting from these advantages, the devices based on random polymer PM6-5% BDT achieved the highest PCE approaching 16.8%, which is much higher than that of the PM6-based devices. Moreover, the devices based on random polymer PM6-5% BDT exhibited excellent device stability after 600 h of continuous illumination.

2. Results and discussion

The synthetic routes of the monomer (2Br-BDT) and the target six random polymers are shown in Scheme S1,† and the structures of the monomer 2Br-BDT were confirmed by ^{1}H NMR spectroscopy (Fig. S2†). The experimental details are provided in the ESI.† These six random polymers can be simply divided into two categories. The BDT-series introduced different molar ratios of BDT units into polymer PM6 (PM6-5%BDT, PM6-10%
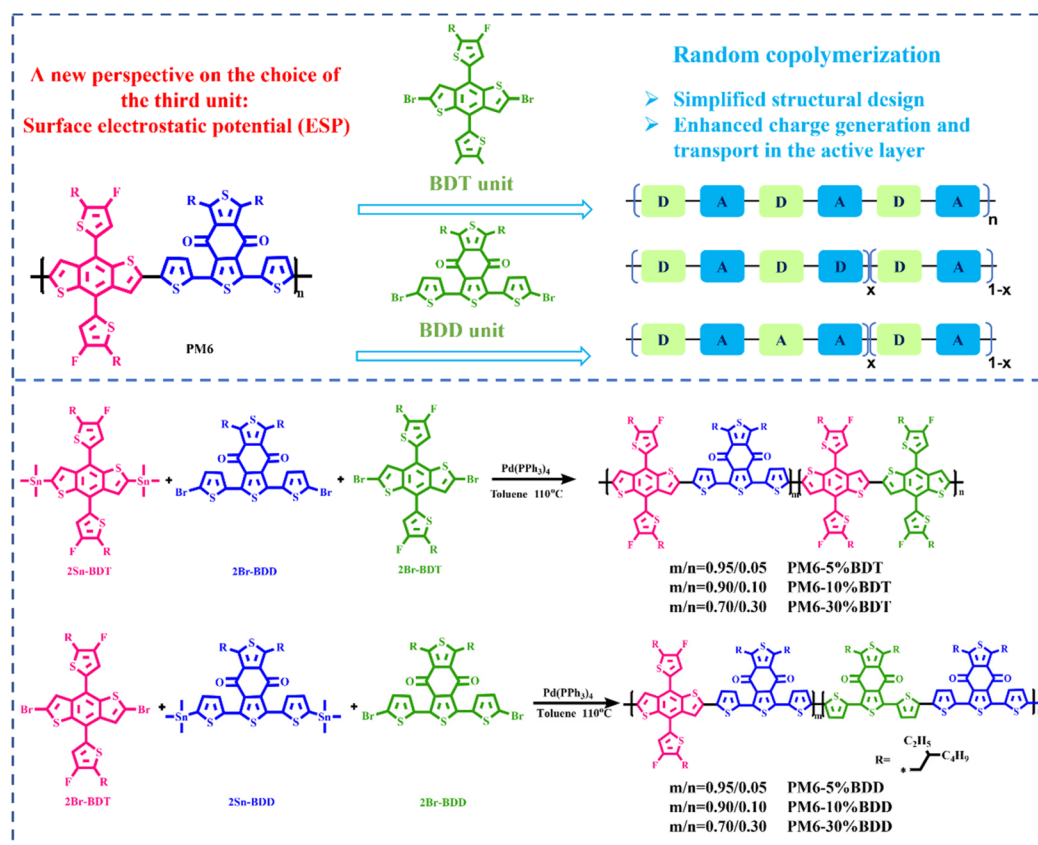

Fig. 1 Synthetic routes and chemical structures of the random polymers.

Table 1 Optical and electrochemical properties of two polymers

Polymer	$\lambda_{max}{}^a$ [nm]	$\lambda_{onset}{}^a$ [nm]	$\lambda_{max}{}^b$ [nm]	$\lambda_{onset}{}^b$ [nm]	$E_g{}^c$ [eV]	HOMO^d [eV]	LUMO^e [eV]	M_n/PDI [kDa]
PM6	618	665	618	680	1.82	−5.63	−3.81	
PM65% BDT	611	666	619	672	1.84	−5.64	−3.80	53.9/1.54
PM6-10% BDT	610	662	616, 577	674	1.84	5.66	−3.82	44.3/1.62
PM6-30% BDT	564	659	566	664	1.87	5.69	−3.82	40.1/1.69
PM6-5% BDD	612	673	618	673	1.84	−5.58	−3.74	43.6/1.96
PM6-10% BDD	612	673	620	680	1.82	−5.56	−3.74	51.5/1.82
PM6-30% BDD	615	688	622	694	1.79	−5.53	−3.74	55.8/1.91

^{a} In chloroform solution. ^{b} In the neat film. ^{c} Calculated from the empirical formula: $E_g = 1240/\lambda_{onset}{}^b$. ^{d} Using the cyclic voltammetry (CV) method. ^{e} Calculated from the equation: $E_{LUMO} = E_{HOMO} + E_g$.

BDT, PM6-30%BDT), while the BDD-series introduced different molar ratios of BDD units into polymer PM6 (PM6-5%BDD, PM6-10%BDD, PM6-30%BDD). The number-average molecular weights (M_ns) of the BDT-series and BDD-series were measured by gel permeation chromatography (GPC), and the details are summarized in Table 1. The six polymers showed a medium M_n value between 40.1 and 55.8 kDa, and the lowest M_n value was achieved for polymer PM6-30%BDT, which may be caused by a too large steric hindrance between the polymerized monomers. In addition, all six polymers showed superior thermal stability with 5% weight loss at temperatures over 300 °C (Fig. S3†).

Density functional theory (DFT) calculations were performed and the changes in the main chain structure of the polymer after the introduction of BDT and BDD units were systematically studied. Firstly, the potential energy surface scans of BDT-BDD, BDT-BDT and BDD-BDD were performed, as shown in Fig. 2a. It can be easily found that those three structures have similar optimal dihedral angles and twisting barriers. However, a slightly higher relative energy emerged in the structures of BDT-BDT and BDD-BDD at 0°, indicating that a more stable molecular configuration was probably formed in those structures. Furthermore, the backbone optimal geometry and surface electrostatic potential (ESP) of two random polymers were also investigated, as shown in Fig. 2b and c, and the details are provided in Fig. S4.† According to the previous report,[40] the molecular surface ESP is defined as the electrostatic potential ($V(r)$) created by the nuclei and electrons of a molecule at each point r in the surrounding space, given rigorously by the following eqn:

$$V(r) = \sum_A \frac{Z_A}{R_A - r} - \int \frac{\rho(r')\mathrm{d}r'}{|r' - r|}$$

where Z_A and R_A denote the nuclear charge and position vector of atom A, respectively. $\rho(r)$ is the molecule's electronic density. As for BDT-series random polymers, similar or even smaller dihedral angles of 0.84° and 4.75° were achieved after the introduction of a BDT unit. What surprises us is that the introduction of such a large structure (BDT unit) does not cause intolerable steric hindrance and destruction of the coplanarity of the backbone. However, increased dihedral angles were observed in BDD-series random polymers after the

introduction of the BDD unit. The different changes in the dihedral angles indicate that the coplanarity of the polymer backbones changes oppositely with the introduction of the third unit. In order to verify the influence of the introduction of the third unit on the distribution of the molecular ESP, the related simulation calculation was performed on these two structures. The results showed that after the introduction of the BDT unit, the molecular structure exhibited a negative electrostatic potential in a very wide area, implying that the interaction between donor and materials could be stronger in blend films, which is beneficial for charge generation and transport. Besides, as shown in Fig. S4c and Table S1,† the results of the dipole moment simulation indicated that a larger component in the direction perpendicular to the molecular plane was observed in the structure of BDT-BDD-BDT-BDT, which may be more favorable for the formation of a face-on orientation. Nevertheless, the direction of the dipole moment in the structure of BDT-BDD-BDD-BDD was parallel to the molecular plane, which is favorable for intermolecular packing.

X-ray diffraction (XRD) analysis was performed to study the crystallinity of neat films, as shown in Fig. 3a. A sharp diffraction peak at around 4.70° to 4.82° was observed in random polymers and PM6 neat films, and it can be easily found that the full width at half maximum (FWHM) values of the PM6-5% BDT and PM6-5%BDD neat films are smaller than that of the PM6 neat film, indicating that the crystallinity of these two random polymers has not been impaired by the random copolymerization process. The highest occupied molecular orbital (HOMO) energy level of the materials was measured by cyclic voltammetry (CV), as shown in Fig. S5,† and the detailed energy level diagrams of random polymers and PM6 are displayed in Fig. 3b. It is obvious that the HOMO energy levels of the random polymers have increased significantly after the introduction of the BDD unit, and it becomes more and more obvious as the number of BDD units introduced increases. Compared to those of the BDD-series random polymers, the HOMO energy levels of the BDT-series random polymers exhibited the opposite result, in which downshifted HOMO levels were obtained after the introduction of the BDT unit. This interesting phenomenon was attributed to the strong electron-deficient effect of F-substitution on the D-unit.[41,42] These results indicate that a smaller HOMO–HOMO offset with the
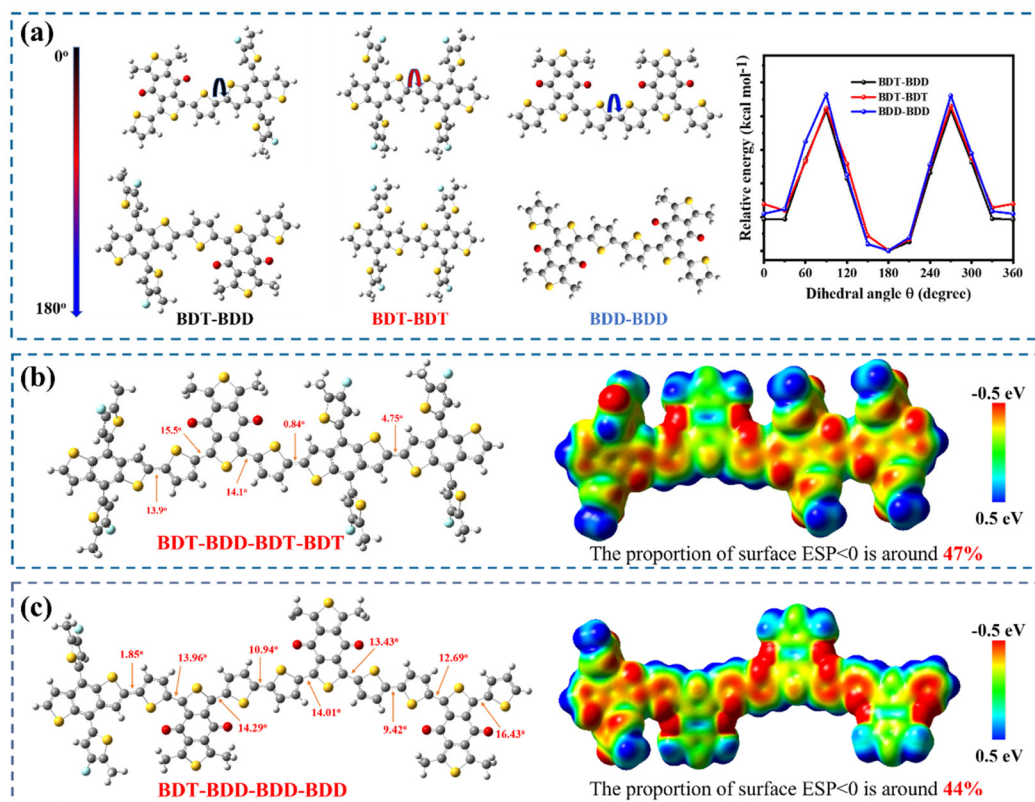
Fig. 2 (a) Potential energy surface scans of the three different connection methods (BDT-BDD, BDT-BDT and BDD-BDD); optimized conformations and the molecular electrostatic potential (ESP) distribution of (b) BDT series random polymers and (c) BDD series random polymers. All of the simulation calculations were based on DFT calculations at the B3LYP/6-31 g(d,p) level and the side chains were replaced with methyl groups.

acceptor Y6 will be more likely formed in the BDT-series random polymers, which could contribute to a higher V_{OC} and smaller energy loss (E_{loss}).

The ultraviolet–visible (UV–vis) absorption properties of the polymers in chloroform were determined, as shown in Fig. 3c. The solution absorption spectra of all the random polymers, except for PM6-30%BDT, are very similar to that of PM6, which showed a maximum absorption peak appearing at about 610 nm. As for PM6-30%BDT, the peak at around 610 nm was much reduced and the maximum absorption peak appeared at 564 nm, which may be attributed to its increased molecular disorder and weakened π–π stacking. In addition, it is obvious that the BDT-series random polymers showed a blue-shifted absorption edge, while an opposite trend was observed in the BDD-series random polymers. The temperature-dependent UV–vis absorption spectra of the polymers in chlorobenzene were also recorded to explore their aggregation properties, as shown in Fig. S6.† According to the previous literature,[43,44] PM6 exhibited a strong temperature-dependent aggregation property, where a significant blue-shift of the absorption can be observed when the temperature increased. However, the temperature-dependent aggregation property was reduced in the random polymers. The weaker temperature-dependent aggregation property in random polymers not only can ensure a room temperature solution process ability, but also can influ-

ence the active layer morphology. On the other hand, the absorption spectra of the polymer neat films were also measured, and similar absorption behaviors have been found, as shown in Fig. 3d. The absorption edge of the polymer film spectra red-shifted when compared with that in solution, and the optical energy bandgaps (E_gs) of the polymers were calculated from their corresponding absorption edges. In summary, the optical and electrochemical properties of the random polymers and PM6 are provided in Table 1.

The photovoltaic properties of random polymers were demonstrated in a conventional device with the structure ITO/PEDOT:PSS/polymer:Y6/PDINO/Al. For comparison, the devices based on PM6:Y6 as the active layer were also fabricated. The current density–voltage (J–V) curves of the devices based on the polymers are shown in Fig. 4a, and the corresponding photovoltaic parameters are summarized in Table 2. The control device based on PM6:Y6 achieved a PCE of 15.65%, with a V_{OC} of 0.85 V and a fill factor (FF) of 72.4%, which was comparable to previous results.[15] Interestingly, the performance of the devices based on random polymers becomes much more complicated. For the ease of comparison, the changing trend of PCE and V_{OC} with the third component content and the PCE distributions are shown in Fig. 4b and c. As for the devices based on the BDT-series polymers, V_{OC} exhibited an increasing trend as the number of BDT units
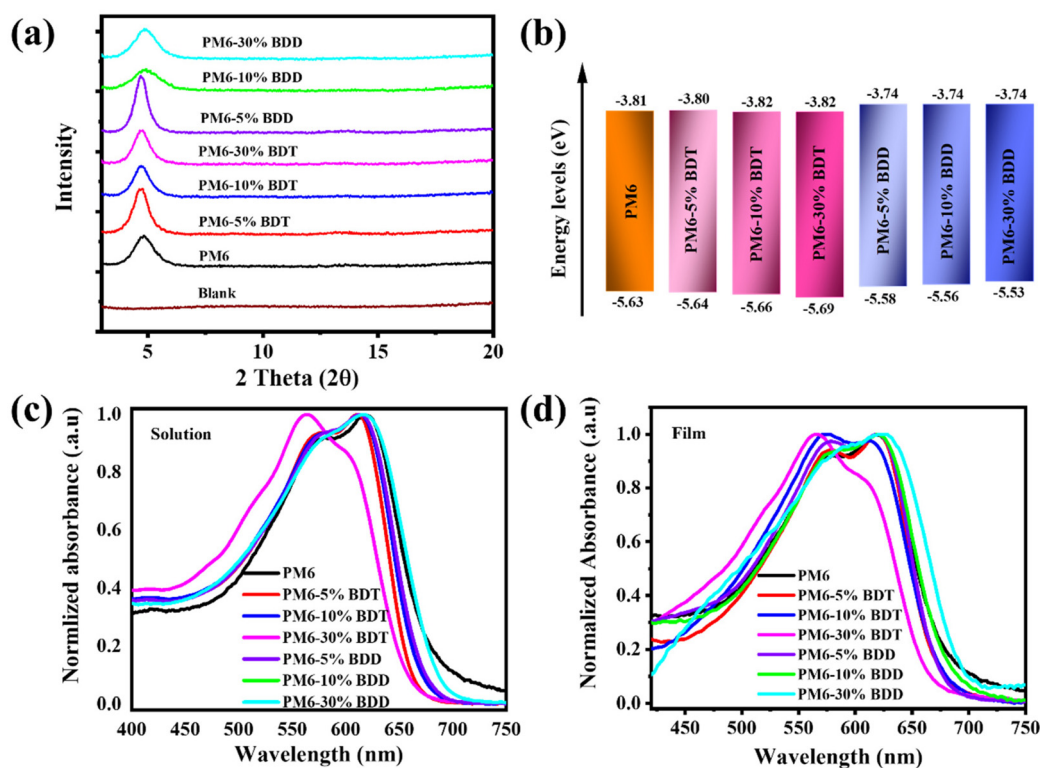
Fig. 3 (a) The XRD scattering patterns of random polymers and PM6 films. (b) Energy level diagrams of the random polymers and PM6; normalized UV−vis absorption spectra (c) in dilute chloroform solution and (d) in thin films of the random polymers and PM6.

increased, which was consistent with the gradually down-shifted HOMO energy levels of the random polymers. However, an obvious change of increase first and then decrease appeared in the short-circuit current density (J_{SC}) and FF of the devices when the number of BDT units increased, which could be caused by the poor morphology of the active layer. As a result, the best-performing device was achieved when the 5% BDT unit was introduced into PM6, which showed an excellent PCE of 16.76%. The improved performance was related to the simultaneous enhancement of V_{OC}, J_{SC} and FF values, especially in terms of J_{SC}, which increased from 25.46 to 25.95 mA cm^{-2}. In comparison, all of the devices based on BDD-series random polymers showed a lower PCE of less than 14%, due to a significant decrease in J_{SC} and FF values. Surprisingly, the V_{OC} values of the devices also increased as the HOMO energy level of the BDD-series random polymers increased, which was attributed to the lower voltage loss (V_{loss}) in these devices.

The external quantum efficiency (EQE) spectra of the corresponding devices are shown in Fig. 4d, and the calculated integrated current densities are presented in Table 2. Similar EQE spectra in the 300–900 nm wavelength region were obtained for these devices and a slightly enhanced EQE response was found from 370 to 440 nm in the random polymer based devices, except for polymer PM6-30%BDD. However, it is obvious that only the device based on PM6-5%BDT showed a comparable EQE response when compared with the control

device, which is consistent with the result that the J_{SC} values of most random polymer based devices are lower than that of the control device. The reduced J_{SC} values of random polymer based devices were deduced to be associated with their lower charge transport efficiency. It should be pointed out that the integrated J_{SC} values agreed well with the measured J_{SC} values. To verify this conjecture, space-charge-limited current (SCLC) measurement was performed to study the charge carrier mobilities of the blend films (Fig. S7† and Fig. 4e). The structure of the test devices and fabrication details are given in the ESI.† The PM6-5%BDT:Y6 blend exhibited the highest hole mobilities (μ_h) and electron mobilities (μ_e) of 7.19×10^{-4} and 5.23×10^{-4} cm^2 V^{-1} s^{-1}, respectively, which are much better than those of the PM6:Y6 blend. The improved mobilities were considered as one of the important factors for the improvement of J_{SC} and FF in the PM6-5%BDT-based device. However, as the amount of BDT units further increased, the blend films based on random polymers showed a decreasing trend. Furthermore, all of the blend films based on BDD-series random polymers displayed a sharp downward trend, where the μ_h value of the blend film decreased from 10^{-4} cm^2 V^{-1} s^{-1} to 10^{-5} cm^2 V^{-1} s^{-1}. Therefore, the poor charge transfer efficiency of the blend films based on BDD-series random polymers leads to a drastic drop in device performance.

The differences in the charge transfer efficiency of devices based on six random polymers and PM6 were fully investigated. First of all, the charge recombination behavior was care-
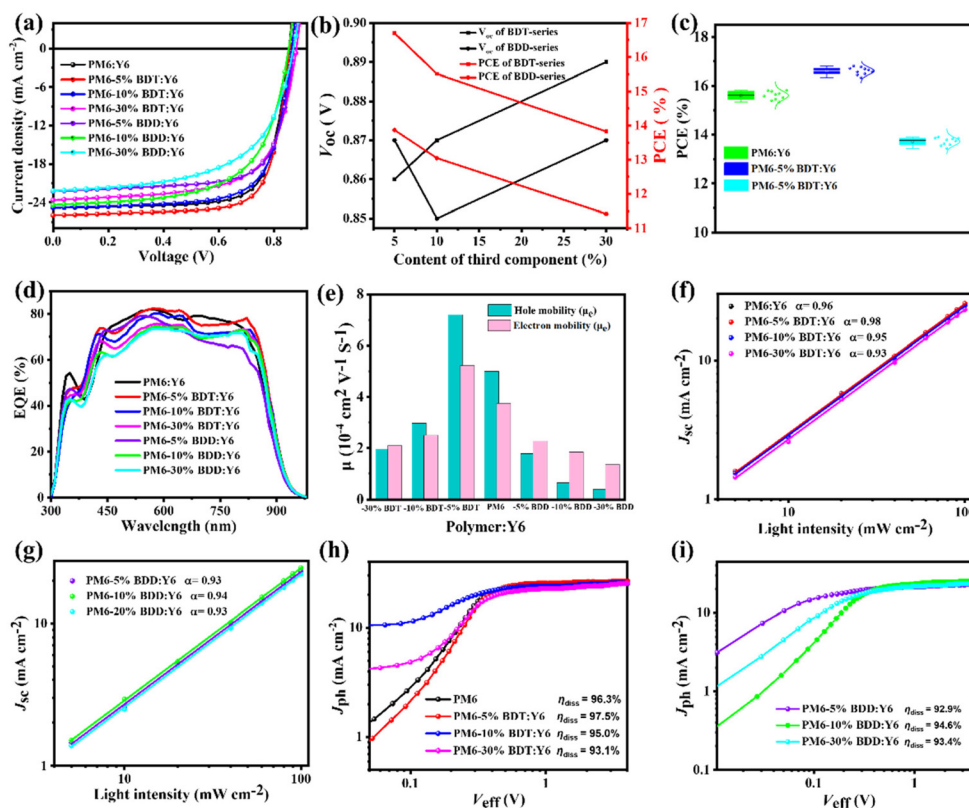
Fig. 4 (a) Current density *versus* voltage (*J*–*V*) curves of organic solar cells based on the random polymers and PM6; (b) the changing trend of PCE and V_{OC} with the content of the third unit; (c) PCE distributions of devices based on the random polymers and PM6; (d) EQE curves of the corresponding optimal devices; (e) electron mobility and hole mobility of the different active layers. (f and g) Light intensity dependence of J_{sc} and (h and i) J_{ph}–V_{eff} curves of the corresponding devices based on the random polymers and PM6.

Table 2 Photovoltaic parameters of the devices based on different polymer donors with the acceptor Y6

Active layer	V_{OC} (V)	J_{SC} (mA cm^{-2})	FF (%)	PCE (%)
PM6	0.85	25.46 (24.30)[a]	72.39	15.65 (15.50 ± 0.13)[b]
PM6-5% BDT	0.86	25.95 (24.68)	75.12	16.76 (16.59 ± 0.20)
PM6-10% BDT	0.87	24.86 (23.98)	71.71	15.51 (15.40 ± 0.18)
PM6-30% BDT	0.89	23.65 (23.18)	66.27	13.83 (13.60 ± 0.25)
PM6-5% BDD	0.87	22.76 (22.59)	71.46	13.87 (13.65 ± 0.22)
PM6-10% BDD	0.85	24.39 (22.74)	62.63	13.05 (12.90 ± 0.16)
PM6-30% BDD	0.87	22.18 (21.90)	59.15	11.42 (11.30 ± 0.12)

[a] The integrated J_{SC} values in parentheses were calculated from the EQE spectra. [b] The average PCEs in parentheses were calculated from 20 devices.

fully explored through the relationship between J_{SC} and the light intensity (*P*), which is described as $J_{SC} \propto P^{\alpha}$, where α is the recombination parameter. Generally, the parameter α being close to 1 indicates weak bimolecular recombination in the device. As shown in Fig. 4f and g, it is obvious that only the devices based on PM6-5%BDT showed an α value very close to 1 compared to that of the devices based on PM6, indicative of weak bimolecular recombination in the PM6-5% BDT based device. The devices based on the other five random polymers showed a lower α value between 0.93 and 0.95, which partly explained the lower J_{SC} and FF values in these devices.

Moreover, the exciton dissociation and charge collection behavior were also investigated through the relationship between the photocurrent density (J_{ph}) and the effective voltage (V_{eff}), as shown in Fig. 4h and i. Furthermore, the exciton dissociation efficiency (η_{diss}) can be estimated from the J_{ph}–V_{eff} curves. After calculation, the PM6-5%BDT based devices achieved a η_{diss} value of 97.5% while for the devices based on PM6 it was 96.3%, and lower η_{diss} values between 95.0% and 92.9% were obtained for the devices based on the other five random polymers. Therefore, due to weak bimolecular recombination and higher exciton dissociation efficiency, the J_{SC} and

FF of the PM6-5%BDT based devices reached the highest values. In addition, efficient fluorescence quenching was also discovered in blend films through steady-state photoluminescence (PL) measurement (Fig. S8†).

Femtosecond transient absorption (fs-TA) spectroscopy measurements were carried out to trace the photoinduced hole transfer process in those blend films. Here, a fs laser of 750 nm was applied to selectively pump Y6 without exciting the donors. In the TA spectra of the neat Y6 film displayed in Fig. S9,† the two bleach peaks that appeared at 620–880 nm were attributed to the ground state bleach (GSB) signal and stimulated emission (SE) signal of Y6. We have also shown the typical TA spectra after 750 nm excitation for PM6-5%BDT:Y6 (Fig. 5a and b), PM6-5%BDD:Y6 (Fig. 5c and d) and PM6:Y6 (Fig. S10†), respectively. Compared with the neat Y6 film, we extracted the normalized kinetics of the new bleach peaks at 605–615 nm with the emergence of the donor's GSB signal (shown in Fig. 5e), suggesting a typical biphasic hole transfer behavior which can be fitted by the biexponential function ($i = A_1 \exp(-t/\tau_1) + A_2 \exp(-t/\tau_2)$). As plotted in Fig. 5f and Table S2,† τ_1 and τ_2 represent the interfacial hole transfer process and NFA exciton diffusion before interfacial dissociation, showing transfer rates as follows: PM6:Y6 ($\tau_1 = 0.148$ ps; $\tau_2 = 16.7$ ps); PM6-5%BDT:Y6 ($\tau_1 = 0.152$ ps; $\tau_2 = 17.8$ ps) and PM6-5%BDD:Y6 ($\tau_1 = 0.149$ ps; $\tau_2 = 21.6$ ps). It is clear that ultrafast interfacial hole transfer (<200 fs) occurred in all three blend films, indicating that the modification of the polymer donor still supplies sufficient driving force for hole transfer. PM6:Y6 and PM6-5%BDD:Y6 systems have similar hole transfer kinetics, but PM6-5%BDD:Y6 has the smallest A_1 and longest τ_2 values, indicating a reduced interfacial charge transfer proportion and a larger Y6 domain for the blend

morphology.[45,46] In this case, more Y6 singlet exciton recombination may occur before dissociation, thus diminishing the hole transfer efficiency, which is in good agreement with the reduction in the EQE and J_{SC} values of the PM6-5%BDD:Y6 based device.

Grazing incidence wide-angle X-ray scattering (GIWAXS) experiments were carried out to investigate the molecular packing characteristics of each of the pure films and blend films, and the detailed data are provided in Table 3. As shown in Fig. 6a–c and g, the neat films of PM6, PM6-5%BDT and PM6-5%BDD demonstrated a preferential face-on orientation, which are beneficial for the improvement of charge transfer in the vertical direction. Besides, an obviously weakened face-on orientation was found in the PM6-5%BDD neat film, in which the orientation preference factor was estimated to be 2.13, while the ratio was 4.94 in the PM6 neat film. It should be noted that the larger the value, the stronger the face-on orientation. Specifically, the PM6 neat film exhibited a strong π–π stacking peak at $q \approx 1.676$ Å^{-1} ($d = 3.749$ Å) in the out-of-plane (OOP) direction, with a crystal coherence length (CCL) of 16.10 Å at the (010) peak. As for PM6-5%BDT and PM6-5%BDD, the π–π stacking peak in the OOP direction was located at 1.676 ($d = 3.749$ Å) and 1.694 Å^{-1} ($d = 3.708$ Å), and the CCL values were calculated and found to be 16.72 and 15.65 Å at the (010) peak in the OOP direction, respectively. Generally, a longer CCL indicates a higher degree of aggregation and higher molecular crystallinity; therefore, it can be presumed that the crystallinity of PM6-5%BDT is slightly stronger than that of PM6. A similar trend also appeared in blend films.

It is easily found that the blend films based on PM6:Y6 or PM6-5%BDT:Y6 exhibited an obvious π–π stacking diffraction peak in the OOP direction, and the face-on orientation was
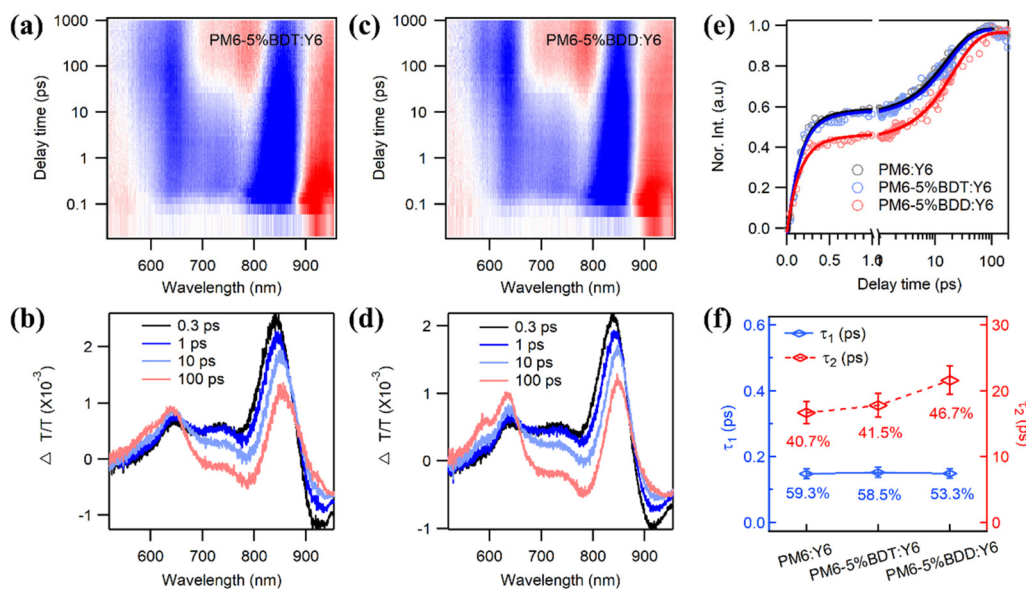

Fig. 5 (a) 2D color plot of fs TA spectra of PM6-5%BDT:Y6 blend films under 750 m excitation. (b) Representative fs TA spectra of PM6-5%BDT:Y6 at indicated delay times. (c) 2D color plot of the fs TA spectra of PM6-5%BDD:Y6 blend films under 750 nm excitation. (d) Representative fs TA spectra of PM6-5%BDD:Y6 at indicated delay times. (e) Hole transfer kinetics and the fitting results. (f) Comparisons of τ_1 and τ_2 of the blends.

Table 3 The data analysis of GIWAXS measurement of pure films and the corresponding blend films

Blend films		Location (Å^{-1})	FWHM (Å)	D-Spacing (Å)	CCL (Å)	Orientation preference factor
PM6	OOP	1.676	0.3512	3.749	16.10	4.941
	IP	0.284	0.1036	22.16	54.56	
		1.696	0.4142	3.704	13.65	
PM6-5%BDT	OOP	1.676	0.3383	3.749	16.72	3.463
	IP	0.2858	0.0890	21.99	63.55	
		1.695	0.3309	3.706	17.09	
PM6-5%BDD	OOP	1.694	0.3613	3.708	15.65	2.125
	IP	0.2893	0.0875	21.72	64.60	
		1.706	0.3809	3.683	14.85	
PM6:Y6	OOP	1.727	0.2357	3.639	23.99	
	IP	0.2096	0.0108	29.98	522.8	
		0.2926	0.0752	21.48	75.20	
		0.4126	0.0850	15.23	66.49	
PM6-5%BDT:Y6	OOP	1.727	0.2456	3.638	23.02	
	IP	0.2153	0.0154	29.18	367.8	
		0.2905	0.0646	21.63	87.55	
		0.4093	0.1117	15.35	50.63	
PM6-5%BDD:Y6	OOP	1.715	0.2378	3.665	23.78	
	IP	0.2904	0.0751	21.63	75.31	
		0.3936	0.1422	15.96	39.78	
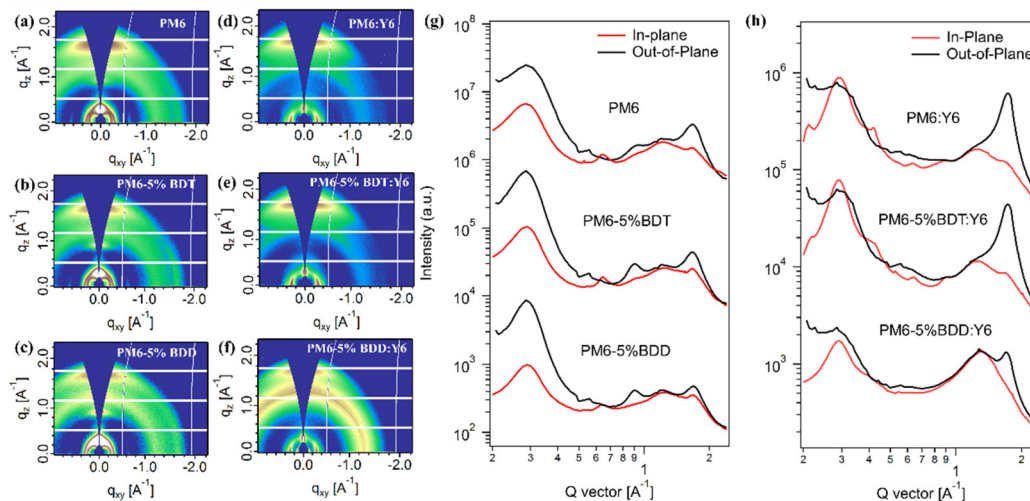
Fig. 6 Two-dimensional GIWAXS patterns of (a) PM6, (b) PM6-5% BDT, (c) PM6-5% BDD, (d) PM6:Y6, (e) PM6-5% BDT:Y6, (f) PM6 PM6-5% BDD:Y6 and (g–f) the one-dimensional integral curves for corresponding films.

even slightly enhanced in the blend film of PM6-5% BDT:Y6 when compared to PM6:Y6, as shown in Fig. 6d–f and h. Interestingly, a new strong diffraction peak emerged in the in-plane (IP) direction of the PM6-5%BDD:Y6 blend film, located at 1.399 Å^{-1}, indicating that a strong lamellar stacking structure existed in the IP direction. Moreover, it is notable that in PM6-5%BDT:Y6 and PM6-5%BDD:Y6 blend films, the CCL values in the IP direction at around 0.29 Å^{-1} were calculated and found to be 87.55 and 75.31 Å, which are larger than that of the PM6:Y6 blend film (75.19 Å). The higher CCL in random polymer-based blend films demonstrated a more orderly mole-cular packing in the IP direction. Moreover, a peak at ~1.3 Å^{-1} in the OOP direction of the PM6-5%BDD:Y6 blend film was found, which statistically reflects the average molecular distance in the amorphous region. In other words, Y6 crystallization in the PM6-5%BDD:Y6 blend is obviously suppressed, with the disappearance of Y6 (020) and (11−1) peaks, which are located at 0.21 and 0.42 Å^{-1} in the IP direction, respectively. It also means that more Y6 molecules enter the amorphous region, the crystalline structure is suppressed, and thus efficient electron transport is difficult to guarantee. This result can be verified by the simulation of the surface electrostatic
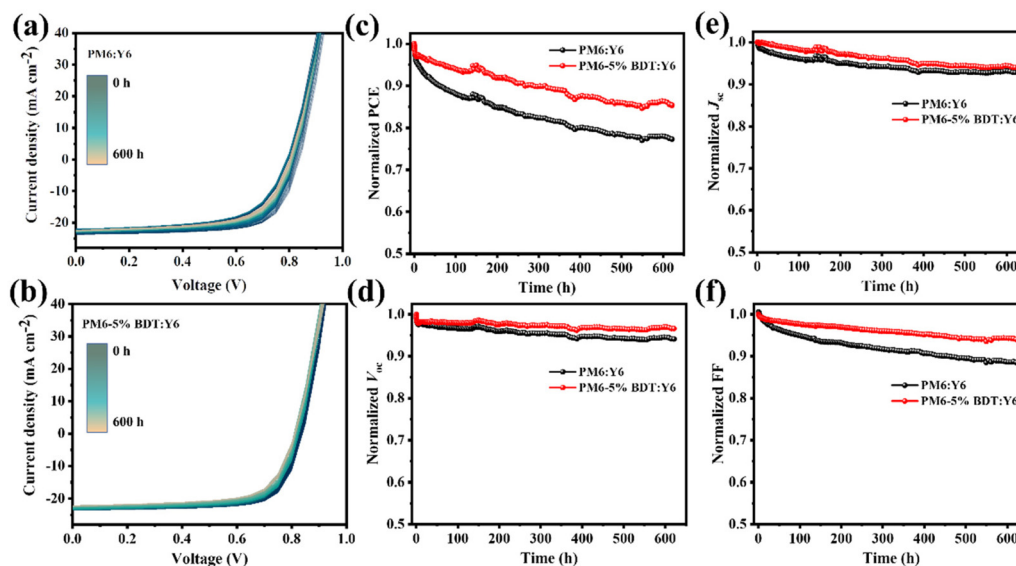
Fig. 7 Photostability of the devices based on polymer PM6 and PM6-5%BDT under a N$_2$ atmosphere, continuous 1-sun-equivalent white LED illumination and room temperature conditions: (a and b) recorded current−voltage curves and photovoltaic parameters as a function of time for devices, (c) PCE, (d) V_{OC}, (e) J_{SC}, and (f) FF.

potential. Compared with PM6-5% BDT, the ESP simulation results of PM6-5% BDD showed that the proportion of surface ESP < 0 is reduced, which means the area of interaction when blending with Y6 will be reduced, thus leading to a weaker electrostatic interaction between the donor and the acceptor, and finally reduces the miscibility between the donor and the acceptor. In addition, the coplanarity of PM6-5% BDD is worse than that of PM6-5% BDT. Therefore, it is believed that PM6-5% BDD in the blend film will break the orderly stacking of Y6, which can also be proved by the larger roughness on the AFM height images later.

Furthermore, the surface morphology of the active layer was examined through atomic force microscopy (AFM) (Fig. S11†). All of the blend films displayed a uniform and smooth surface morphology, while some changes appeared after the incorporation of different third units into polymer PM6. The PM6:Y6 blend film showed a smooth surface with a small root-mean-square (RMS) roughness of 1.22 nm, which is in good agreement with previous reports. As for the blend films based on BDT series random polymers, the roughness values increased as the content of BDT units increased, from 1.12 to 1.64 nm. Although there is no obvious changing trend in the roughness values of the blend films based on BDD series random polymers, it can be easily found that a more obvious phase separation occurred in the PM6-30%BDD:Y6 blend film, which was considered to be caused by aggregation enhancement, and also agreed well with the results of GIWAXS measurements. Moreover, the transmission electron microscopy (TEM) images also showed similar phenomena. As shown in Fig. S12,† the difference of those blend films appeared in the PM6-30%BDD:Y6 blend film because of the greater phase separation, which had been observed in AFM measurements. The poor phase-separation morphology of the PM6-30%BDD:Y6 blend film

thus results in serious exciton recombination and decreased charge separation and transport efficiency.

To meet the requirements of industrial commercialization, device stability, as a key parameter, should be taken into consideration. Herein, the photostability of the devices based on polymer PM6 and PM6-5%BDT under continuous LED illumination and at room temperature was tested. The stability data were collected from twelve devices measured under the same aging conditions. The degradation trend of the device parameters (PCE, J_{SC}, V_{OC} and FF) is presented in Fig. 7, which showed that the devices based on PM6-5%BDT achieved much better stability than the control devices. As for the degradation of PCE, a slower decreasing trend retaining 85% of the initial PCE after 600 h was observed in the devices based on PM6-5% BDT, while about 25% of the initial PCE was lost in the devices based on PM6. The degradation in PCE is mainly from FF and V_{OC} losses, especially FF losses. It can be easily seen that more rapid decay of the FF occurred in the devices based on PM6, with 12% of the initial FF lost after 600 h, which was much larger than that of the PM6-5%BDT-based devices (5%). Besides, a slight quickly decreasing trend of V_{OC} was also found in the devices based on PM6. These results demonstrate that the OSC devices based on random polymers can still achieve better stability performance.

3. Conclusion

In conclusion, a series of BDT and BDD based random polymers were prepared by adopting the random copolymerization strategy to introduce unequal amounts of BDT units and BDD units into the molecular structure of polymer PM6, respectively. This nonequivalent design strategy induced obvious

regulation effects on the absorption spectra and energy levels of the polymers. Complementary absorption spectra and well-matched energy level structures were observed for the BDT series random polymers, while the changing trend is reversed in the BDD series random polymers. Due to the higher charge transport efficiency and lower bimolecular recombination, a highest PCE of 16.76% was obtained for the PM6-5%BDT:Y6 based device, which was much higher than that of the control device. In comparison, the performance of the devices based on the BDD series random polymers showed a trend of sharp decline, which was mainly attributable to the significantly worsened molecular packing, thereby resulting in reduced charge transport efficiency. Moreover, the PM6-5%BDT:Y6 based devices exhibited excellent device stability after 600 h of continuous illumination. This work demonstrated that the strategy of using the same structural unit of PM6 to modify polymers through random copolymerization is an effective method to achieve highly efficient OSCs with better stability, and provides an important reference for developing efficient polymer donors in the future.

Conflicts of interest

The authors declare no conflict of interest.

Acknowledgements

References

1 A. J. Heeger, *Adv. Mater.*, 2014, **26**, 10–28.
2 W. Liu, X. Xu, J. Yuan, M. Leclerc, Y. Zou and Y. Li, *ACS Energy Lett.*, 2021, **6**, 598–608.
3 H. Gaspar, G. Bernardo and A. Mendes, *Nanoenergy Adv.*, 2022, **2**, 1–28.
4 R. Yu, X. Wei, G. Wu and Z. Tan, *Aggregate*, 2022, **3**, 1–21.
5 Y. Liu, J. Zhao, Z. Li, C. Mu, W. Ma, H. Hu, K. Jiang, H. Lin, H. Ade and H. Yan, *Nat. Commun.*, 2014, **5**, 1–8.
6 G. Xu, H. Rao, X. Liao, Y. Zhang, Y. Wang, Z. Xing, T. Hu, L. Tan, L. Chen and Y. Chen, *Chin. J. Chem.*, 2020, **38**, 1553–1559.
7 G. Xu, X. Hu, X. Liao and Y. Chen, *Chin. J. Polym. Sci.*, 2021, **39**, 1441–1447.
8 K. Chong, X. Xu, H. Meng, J. Xue, L. Yu, W. Ma and Q. Peng, *Adv. Mater.*, 2022, **34**, 2109516.
9 D. Chen, S. Liu, X. Hu, F. Wu, J. Liu, K. Zhou, L. Ye, L. Chen and Y. Chen, *Sci. China: Chem.*, 2022, **65**, 182–189.
10 J. Wang, M. Zhang, J. Lin, Z. Zheng, L. Zhu, P. Bi, H. Liang, X. Guo, J. Wu, Y. Wang, L. Yu, J. Li, J. Lv, X. Liu, F. Liu, J. Hou and Y. Li, *Energy Environ. Sci.*, 2022, **15**, 1585–1593.
11 X. Liao, Q. Xie, Y. Guo, Q. He, Z. Chen, N. Yu, P. Zhu, Y. Cui, Z. Ma, X. Xu, H. Zhu and Y. Chen, *Energy Environ. Sci.*, 2022, **15**, 384–394.
12 Y. Cui, Y. Xu, H. Yao, P. Bi, L. Hong, J. Zhang, Y. Zu, T. Zhang, J. Qin, J. Ren, Z. Chen, C. He, X. Hao, Z. Wei and J. Hou, *Adv. Mater.*, 2021, **33**, 2102420.
13 X. Liao, F. Wu, Y. An, Q. Xie, L. Chen and Y. Chen, *Macromol. Rapid Commun.*, 2017, **38**, 1600556.
14 X. Liao, J. Wang, S. Chen, L. Chen and Y. Chen, *Chin. J. Polym. Sci.*, 2016, **34**, 491–504.
15 J. Yuan, Y. Zhang, L. Zhou, G. Zhang, H.-L. Yip, T.-K. Lau, X. Lu, C. Zhu, H. Peng, P. A. Johnson, M. Leclerc, Y. Cao, J. Ulanski, Y. Li and Y. Zou, *Joule*, 2019, **3**, 1140–1151.
16 D. Luo, W. Jang, D. D. Babu, M. S. Kim, D. H. Wang and A. K. K. Kyaw, *J. Mater. Chem. A*, 2022, **10**, 3255–3295.
17 Z. Xiao, X. Jia, D. Li, S. Wang, X. Geng, F. Liu, J. Chen, S. Yang, T. P. Russel and L. Ding, *Sci. Bull.*, 2017, **62**, 1494–1496.
18 Y. Cui, H. Yao, J. Zhang, K. Xian, T. Zhang, L. Hong, Y. Wang, Y. Xu, K. Ma, C. An, C. He, Z. Wei, F. Gao and J. Hou, *Adv. Mater.*, 2020, **32**, 1908205.
19 K. Jiang, Q. Wei, J. Y. L. Lai, Z. Peng, H. K. Kim, J. Yuan, L. Ye, H. Ade, Y. Zou and H. Yan, *Joule*, 2019, **3**, 3020–3033.
20 C. Li, J. Zhou, J. Song, J. Xu, H. Zhang, X. Zhang, J. Guo, L. Zhu, D. Wei, G. Han, J. Min, Y. Zhang, Z. Xie, Y. Yi, H. Yan, F. Gao, F. Liu and Y. Sun, *Nat. Energy*, 2021, **6**, 605–613.
21 J.-W. Lee, D. Jeong, D. J. Kim, T. N-L. Phan, J. S. Park, T.-S. Kim and B. J. Kim, *Energy Environ. Sci.*, 2021, **14**, 4067–4076.
22 Y. Luo, X. Wang, C. Xiao, Z. Li, S. Lei, Y. Yu, B. Xiao, Z. Liu and R. Yang, *ACS Appl. Energy Mater.*, 2021, **4**, 13110–13119.
23 B. Huang, X. Deng, H. Jin, K. Liu, S. Chen, Z. Ma, J. Oh, C. Yang, J. Liu and L. Chen, *J. Mater. Chem. A*, 2022, **10**, 18714–18722.
24 M. Jeong, J. Oh, Y. Cho, B. Lee, S. Jeong, S. M. Lee, S.-H. Kang and C. Yang, *Adv. Funct. Mater.*, 2021, **31**, 2102371.
25 J. Zhang, Q. Huang, K. Zhang, T. Jia, J. Jing, Y. Chen, Y. Li, Y. Chen, X. Lu, H. Wu, F. Huang and Y. Cao, *Energy Environ. Sci.*, 2022, **15**, 4561–4571.
26 J.-W. Lee, S. Seo, S.-W. Lee, G.-U. Kim, S. Han, T. N. Phan, S. Lee, S. Li, T.-S. Kim, J.-Y. Lee and B. J. Kim, *Adv. Mater.*, 2022, 2207544.
27 Y. Li, Q. Li, Y. Cai, H. Jin, J. Zhang, Z. Tang, C. Zhang, Z. We and Y. Sun, *Energy Environ. Sci.*, 2022, **15**, 3854–3861.
28 X. Liu, C. Zhang, C. Duan, M. Li, Z. Hu, J. Wang, F. Liu, N. Li, C. J. Brabec, R. A. J. Janssen, G. C. Bazan, F. Huang and Y. Cao, *J. Am. Chem. Soc.*, 2018, **140**, 8934–8943.

29 L. Huo, X. Xue, T. Liu, W. Xiong, F. Qi, B. Fan, D. Xie, F. Liu, C. Yang and Y. Sun, *Chem. Mater.*, 2018, **30**, 3294–3300.

30 Z. Li, X. Xu, W. Zhang, X. Meng, W. Ma, A. Yartsev, O. Inganäs, M. R. Andersson, R. A. J. Janssen and E. Wang, *J. Am. Chem. Soc.*, 2016, **138**, 10935–10944.

31 S. Chen, H. J. Cho, J. Lee, Y. Yang, Z.-G. Zhang, Y. Li and C. Yang, *Adv. Energy Mater.*, 2017, **21**, 1701125.

32 M. Jeong, S. Chen, S. M. Lee, Z. Wang, Y. Yang, Z.-G. Zhang, C. Zhang, M. Xiao, Y. Li and C. Yang, *Adv. Energy Mater.*, 2017, **8**, 1702166.

33 H. Sun, T. Liu, J. Yu, T.-K. Lau, G. Zhang, Y. Zhang, M. Su, Y. Tang, R. Ma, B. Liu, J. Liang, K. Feng, X. Lu, X. Guo, F. Gao and H. Yan, *Energy Environ. Sci.*, 2019, **12**, 3328–3337.

34 D. Chen, J. Yao, L. Chen, J. Yin, R. Lv, B. Huang, S. Liu, Z. Zhang, C. Yang, Y. Chen and Y. Li, *Angew. Chem., Int. Ed.*, 2018, **57**, 4580–4584.

35 T. Wang, R. Sun, M. Shi, F. Pan, Z. Hu, F. Huang, Y. Li and J. Min, *Adv. Energy Mater.*, 2020, **10**, 2000590.

36 L. Ma, S. Zhang, J. Zhu, J. Wang, J. Ren, J. Zhang and J. Hou, *Nat. Commun.*, 2021, **12**, 5093–5105.

37 H. Chen, Y. Zou, H. Liang, T. He, X. Xu, Y. Zhang, Z. Ma, J. Wang, M. Zhang, Q. Li, C. Li, G. Long, X. Wan, Z. Yao and Y. Chen, *Sci. China: Chem.*, 2022, **65**, 1362–1373.

38 L. Ma, H. Yao, J. Wang, Y. Xu, M. Gao, Y. Zu, Y. Cui, S. Zhang, L. Ye and J. Hou, *Angew. Chem., Int. Ed.*, 2021, **60**, 15988–15994.

39 Y. Cui, P. Zhu, X. Shi, X. Liao and Y. Chen, *J. Phys. Chem. C*, 2021, **125**, 10250–10259.

40 D. Hu, Q. Yang, Y. Zheng, H. Tang, S. Chung, R. Singh, J. Lv, J. Fu, Z. Kan, B. Qin, Q. Chen, Z. Liao, H. Chen, Z. Xiao, K. Sun and S. Lu, *Adv. Sci.*, 2021, **8**, 2004262.

41 J-Y. Kim, S. Park, S. Lee, H. Ahn, S-Y. Joe, B. J. Kim and H. J. Son, *Adv. Energy Mater.*, 2018, **8**, 1801601.

42 Z. Shang, L. Zhou, C. Sun, L. Meng, W. Lai, J. Zhang, W. Huang and Y. Li, *Sci. China: Chem.*, 2021, **64**, 1031–1038.

43 S. Zhang, Y. Qin, J. Zhu and J. Hou, *Adv. Mater.*, 2018, **30**, 1800868.

44 Y. Zhang, L. Pan, Z. Peng, W. Deng, B. Zhang, X. Yuan, Z. Chen, L. Ye, H. Wu, X. Gao, Z. Liu, C. Duan, F. Huang and Y. Cao, *J. Mater. Chem. A*, 2021, **9**, 13522–13530.

45 Z. Chen, X. Chen, B. Qiu, G. Zhou, Z. Jia, W. Tao, Y. Li, Y. M. Yang and H. Zhu, *J. Phys. Chem. Lett.*, 2020, **11**, 3226–3233.

46 N. Yao, J. Wang, Z. Chen, Q. Bian, Y. Xia, R. Zhang, J. Zhang, L. Qin, H. Zhu, Y. Zhang and F. Zhang, *J. Phys. Chem. Lett.*, 2021, **12**, 5039–5044.